HHS Public Access

Author manuscript

Acad Radiol. Author manuscript; available in PMC 2020 March 01.

Published in final edited form as:

Acad Radiol. 2019 March ; 26(3): 326–334. doi:10.1016/j.acra.2018.05.025.

Probing changes in lung physiology in COPD using CT, perfusion MRI and hyperpolarized xenon-129 MRI

Kun Qing[1], **Nicholas J. Tustison**[1], **John P Mugler III**[1], **Jaime F. Mata**[1], **Zixuan Lin**[1], **Li Zhao**[2], **Da Wang**[3], **Xue Feng**[1], **Ji Young Shin**[1], **Sean J. Callahan**[1], **Michael P. Bergman**[1], **Kai Ruppert**[4], **Talissa A. Altes**[1,5], **Joanne M. Cassani**[1,5], and **Y Michael Shim**[1]

[1]University of Virginia

[2]Beth Israel Deaconess Medical Center

[3]University of Washington

[4]University of Pennsylvania

[5]University of Missouri

Abstract

Rationale and Objectives: COPD is highly heterogeneous and not well understood. Hyperpolarized xenon-129 MRI provides a unique way to assess important lung functions such as gas uptake. In this pilot study, we exploited multiple imaging modalities, including CT, gadoliniumenhanced perfusion MRI, and xenon-129 MRI, to perform a detailed investigation of changes in lung morphology and functions in COPD. Utility and strengths of xenon-129 MRI in assessing COPD were also evaluated against the other imaging modalities.

Materials and Methods: Four COPD patients and four age-matched normal (AMN) subjects participated in this study. Lung tissue density measured by CT, perfusion measures from gadolinium-enhanced MRI, and ventilation and gas uptake measures from xenon-129 MRI were calculated for individual lung lobes to assess regional changes in lung morphology and function, and to investigate correlations among the different imaging modalities.

Results: No significant differences were found for all measures among the five lobes in either the COPD or AMN group. Strong correlations ($R>0.5$ or <-0.5, $P<0.001$) were found between ventilation and perfusion measures. Also gas uptake by blood as measured by xenon-129 MRI showed strong correlations with CT tissue density and ventilation measures ($R>0.5$ or <-0.5, $P<0.001$) and moderate to strong correlations with perfusion measures ($R>0.4$ or <-0.5, $P<0.01$). Four distinctive patterns of functional abnormalities were found in patients with COPD.

Conclusions: Xenon-129 MRI has high potential to uniquely identify multiple changes in lung physiology in COPD using a single breath-hold acquisition.

Keywords

Hyperpolarized xenon-129 MRI; CT; perfusion; ventilation; gas exchange

INTRODUCTION

Chronic Obstructive Pulmonary Disease (COPD) is a leading cause of death and disability around the world. Clinical diagnosis and prognosis of COPD are still primarily based on irreversible airflow limitation measured by spirometry. However, multiple studies reported heterogeneous phenotypes of COPD that are far more complicated than being simply defined by irreversible airflow limitation (1–3). Loss of lung function and abnormalities of gas exchange develop early (4) and increase in prevalence as the severity of COPD increases (5). Chronic hypoxemia was reported to be closely related to decline in the patient's quality of life, reduced exercise tolerance, and greater risk of death (6).

There are numerous unanswered questions about the mechanisms of hypoxemia in COPD. Whether hypoxemia is merely caused by ventilation-perfusion (V/Q) mismatch or diffusion impairment is unclear (6, 7). Conventional imaging techniques such as computed tomography (CT) and nuclear medicine scans, have limitations in the assessment of COPD. For example, chest CT provides detailed information about changes in lung morphometry, such as emphysema, bronchiectasis (8), but limited information about lung function. Dual energy chest CT scan can provide iodine distribution maps, which can be used as a surrogate for pulmonary perfusion (9). Nuclear medicine V/Q scan quantifies ventilation and perfusion (10), but with limited spatial and temporal resolution. In addition, pulmonary function testing (PFT) provides whole lung measurements of lung function, but lacks regional localization of abnormalities. Therefore, reliable, non-invasive imaging techniques that can offer detailed assessment and accurate quantification of regional lung function will not only promote the understanding of the pathophysiology of COPD, but will also provide directions for treatment and valuable information about prognosis.

Hyperpolarized xenon-129 (Xe129) dissolved phase (DP) MRI is a new imaging method that permits 3D regional mapping of both ventilation (airflow) and gas uptake by tissue and blood (gas exchange) in the human lung through a single breath hold acquisition (11–13). It is a non-invasive imaging method without ionizing radiation. Multiple outcome measurements can be produced from this method, and are sensitive to important pulmonary physiological factors such as alveolar tissue density, surface-to-volume ratio, pulmonary ventilation, perfusion and gas-blood barrier thickness (14, 15). These properties make it an ideal tool to investigate COPD. However, direct assessment of vasculature is desired to further validate findings from gas exchange parameters obtained by the hyperpolarized Xe129 DP MRI.

In our pilot study, multiple imaging methods (chest CT, perfusion MRI, ventilation and gas uptake MRI) were administered to investigate the *in vivo* pulmonary physiology of patients with COPD. Administration of MR contrast agents via two distinctive routes, inhalation of hyperpolarized Xe129 and intravenous infusion of gadolinium (Gd), enabled us to obtain more complete physiologic parameters of the lung. Data from these imaging methods were

further refined by our analytical approaches to interrogate the results in each anatomic lobe. These experimental and analytic approaches enabled us to describe pulmonary pathophysiology of patients with COPD that was clearly differentiated from healthy controls. They also demonstrated that a given subject with a diagnosis of COPD could exhibit several, diverse pathologic changes including “pulmonary shunt” and “dead space”. Therefore, our study demonstrated potential of using these multiple imaging modalities to increase our ability to better characterize complex phenotypes of COPD in patients.

MATERIALSAND METHODS

Human Subjects

Four patients with COPD and four age-matched normal (AMN) subjects were recruited, and each participant signed written informed consent before the study. COPD patients were categorized according to the GOLD severity classification (16). Criteria for inclusion of COPD patients were: physician diagnosis of COPD, clinically stable to participate in the study and smoking history >10 packs/year. Normal subjects were defined as people who currently feel well with normal spirometry and without respiratory symptoms, an absence of a history of lung disease and a smoking history of less than 100 cigarettes in their life. Subjects with FEV_1 %predicted of less than 25%, or unable to hold their breath for 10 seconds, were excluded from the study. Similarly, since Gd-enhanced perfusion scans were included, exclusion criteria included a glomerular filtration rate of less than 45 ml/min/1.73 m^2 based on creatinine drawn within 30 days of MRI or known hypersensitivity to Gd contrast agents. Each subject underwent pulmonary function tests (PFTs), including spirometry with and without bronchodilator, diffusion capacity for carbon monoxide (DLCO), and six minute walk (6MW). All subjects also completed chest CT, Gd-enhanced perfusion MRI, and hyperpolarized Xe129 MRI. All MRI studies were done on the same day. PFTs and CT scans were done within a 3-day window of the MRI studies for each subject.

Image Acquisitions:

Computed Tomography: Chest CT was done based on the COPDGene protocol (17). Subjects were coached to breathe after maximal inhalation to total lung capacity and hold their breath for about 3–6 seconds depending on the size of the lung. The CT scan was acquired using a SOMATOM Definition Flash (Siemens Healthcare, Forchheim, Germany) at 120 KV, and 200 mAs. The in-plane spatial resolution was approximately 1×1 mm and the slice thickness was 0.75 mm.

Gd-enhanced Perfusion MRI—All MR acquisitions were done using a 1.5T commercial whole-body MR scanner (Avanto; Siemens Medical Solutions, Malvern PA), and spine and body-array RF coils. Gd-DTPA *(gadolinium-based* MRI contrast agent) was injected at the standard dose (0.2ml/kg body weight), simultaneously with data acquisition. A three-dimensional (3D) T1-weighted gradient-echo pulse sequence with echo sharing (Siemens, TWIST) was used to acquire a four-dimensional data set with a real temporal resolution of 1.6–2 seconds, depending on the size of the lung (28 series total), during free breathing. Perfusion image resolution was 2×2×6 mm^3, and total acquisition time was approximately 1

minute using a parallel-imaging acceleration (GRAPPA) factor of 2. Other sequence parameters were TE/TR= 0.78/2.27 ms, flip angle = 25°, bandwidth = 700 Hz/pixel. View sharing was applied to achieve a virtual temporal resolution of 0.8–1 second. The central region was defined as 28% of k-space and sampled at a density of 50% (18). The time to center was 3.3–3.5 seconds.

Combined Hyperpolarized Xe129 and Proton MRI: A combined hyperpolarized gas and proton MR acquisition during a single breath hold provides complementary functional and anatomical information of the lung and facilitates quantification of functional images (19). In this study, each participant underwent this acquisition, which in a single breath hold provides 3D images of Xel29 in pulmonary airspaces (“gas”), interstitial parenchyma and plasma (“tissue”), and red blood cells (RBCs) (11), and also 3D proton images covering the whole lung. The Xel29 acquisition time was approximately 10 seconds at a spatial resolution of $7.6 \times 7.6 \times 17\ mm^3$. The 3D proton pulse sequence, which was appended to the Xe129 dissolved-phase acquisition, had an acquisition time of approximately 3 seconds using acceleration factor of three (20) at an isotropic resolution of about 4 mm. So the total acquisition time for combined Xe129 dissolved-phase and proton MR acquisition was less than 15 seconds. A flexible, circularly-polarized, vest-shaped chest RF coil (Clinical MR Solutions, Brookfield, WI) was used for all Xe129 MRI acquisitions; proton acquisitions used the scanner’s body RF coil. Enriched xenon gas (87% Xe129) was polarized using a Polarean 9820 system (Polarean, Durham, NC) to polarization level between 25% and 40%. Each subject breathed in up to 1 liter of Xe129 mixed with nitrogen to a total volume of 1/3 of their FVC based on spirometry results obtained right before the imaging study.

Imaging Post-processing:

Computed Tomography: Lung regions were divided into five lobes based on the detection of lung fissures (21). The bottom 15^{th} percentile (Perc15) of the CT Hounsfield Unit (HU) numbers was calculated for each lobe to represent the average severity of emphysema in the lobe (22–24).

Gd-enhanced Perfusion MRI: First-pass dynamic Gd-enhanced images of the lung were processed as described in (25) based on indicator dilution theory (26, 27) to determine the quantitative total value of pulmonary perfusion. Three perfusion parameters, i.e., pulmonary blood volume (PBV), pulmonary blood flow (PBF), and mean transit time (MTT), were calculated on a pixel-by-pixel basis for assessment of regional pulmonary perfusion. The arterial input function (AIF) was obtained based on the signal intensity of the main pulmonary artery trunk. To quantitatively compare regional information obtained by different imaging methods, a recently developed lobar segmentation method for proton MRI was applied to the perfusion data (21). The mask for the whole lung was reviewed and adjusted manually for each subject to ensure the accuracy of segmentation. Mean PBV, PBF and MTT values in individual lobes were calculated for each subject.

Combined Hyperpolarized Xe129 and Proton MRI: From the combined Xe129/ proton MR acquisition, four image sets were obtained simultaneously in a single breath hold: Xel29 “gas” images reflecting ventilation, Xel29 “tissue” images reflecting gas uptake

by interstitial lung tissue and plasma, Xel29 RBC images reflecting gas uptake by RBCs in the blood, and also proton images of the lung anatomy. Two quantification methods were used to extract different functional information from this acquisition. First, to determine airflow limitation by measuring dead-space ventilation, lung regions were segmented based on signal intensity of the "gas" ventilation images to non-ventilated, hypo-ventilated, ventilated, and well-ventilated regions (28). The percentage of the lung with abnormally reduced ventilation ($\%V_d$) was calculated as the sum of the non-ventilated and hypo-ventilated volumes normalized to the total lung volume. Second, gas uptake images of the lung were generated as described in (11). Three ratio maps (tissue-to-gas, RBC-to-tissue and RBC-to-gas) are produced from the Xel29 images for quantitative comparison among subjects. The resulting calculated ratios are closely related to important lung physiological factors: the tissue-to-gas ratio mainly reflects tissue density and alveolar surface-to-volume ratio, the RBC-to-tissue ratio is affected by pulmonary perfusion and gas-blood barrier thickness while the RBC-to-gas ratio represents the overall gas exchange efficiency from lung airspaces to the blood, similar to what DLCO measures globally. Different from previous work (11, 12), gas uptake measurements including tissue-to-gas, RBC-to-gas and RBC-to-tissue in lung regions (defined by lung mask obtained from proton images acquired in the same breath hold) with no ventilation were defined as zero for this work, while regions with ventilation were assigned values calculated based on the description in (11).

The accelerated proton images of the lung (via undersampling) were reconstructed using compressed sensing as described in (29). The lobar segmentation method (21) was used to divide the proton images, acquired in the same breath hold as Xe129 images, into individual lung lobes. This segmentation information was then applied to the Xel29 images and ratio maps to determine gas uptake information for each lobe.

Data Analysis:

Features of the two study groups were compared using the Mann-Whitney two-tailed t-Test for scaled continuous data and the Chi Square distribution for categorical data. The Kruskal-Wallis test was performed to compare the five lobes of the lung for different measurements. Correlations among different acquisitions and/or measurements were tested with Pearson correlation analysis. Due to the limited number of subjects recruited in this study, statistical analysis was only performed for lobar mean data, and not for whole-lung mean data. A p-value less than 0.05 was considered statistically significant.

Institutional Review Board

The study was performed under a physician's Investigational New Drug application for hyperpolarized Xel29 MRI using a protocol approved by the Institutional Review Board of our institute.

RESULTS

Subject Features

Subject demographics, PFT and 6MW results are shown in Table 1. Gold stage was assessed based upon the post bronchodilator spirometry. Within the four COPD patients, three of

them (C1-C3) were GOLD stage 2, and one (C4) GOLD stage 4. Significantly lower FEV_1/FVC, FEV_1 %Pred, and DLCO %Pred were noted in the patients with COPD as anticipated.

Global and Regional Differences in Lung Function

Global Evaluation—Whole-lung mean metrics were calculated from the results of different imaging acquisitions. As shown in Table 2, COPD subjects had overall lower CT Percl5 values and lower Xel29 gas uptake measurements, including tissue-to-gas, RBC-to-gas and RBC-to-tissue ratios and higher $\%V_d$ values than healthy volunteers.

Lobar Evaluation—Mean values of the different measurements in individual lobes were calculated based on lobar segmentation of CT and MR images (Table 3). Figure 1 shows representative lobar segmentation for CT and MR images/maps for a slice from subject H4. For the Xel29 MRI results (left column of images), it can be seen that since the Xel29 MR images were acquired in the same breath hold as the proton images, both the ventilation ("gas") image and the generated tissue-to-gas ratio map align with the proton images very well. No within-group statistical difference among lobes was observed for any of the imaging measurements in either the AMN or COPD subjects ($P>0.05$). However, comparing between groups, COPD subjects had significantly lower CT Perc15 ($P<0.001$), MRI perfusion measurement PBF ($P=0.047$), and Xe129 gas uptake measurements including tissue-to-gas, RBC-to-gas and RBC-to-tissue ratios ($P<0.001$). Also the $\%V_D$ in COPD subjects was significantly higher than that in the AMN group ($P=0.006$).

Correlations and Differences among Different Imaging Measurements

Correlations of lobar mean values from different imaging measurements are shown in Table 4. CT Perc15 had strong correlations with Xe129 tissue-to-gas ($R=0.74$, $P<0.001$) and RBC-to-gas ratios ($R=0.62$, $P<0.001$). CT Perc15 correlated moderately with PBV ($R=0.38$, $P=0.016$), PBF ($R=0.38$, $P=0.016$), MTT ($R=-0.36$, $P=0.022$) and $\%V_D$ ($R=-0.33$, $P=0.04$). MRI perfusion measurements correlated significantly with all Xe129 MRI measurements, most strongly with the Xe129 $\%V_D$ (PBV: $R=-0.59$, $P<0.001$; PBF: $R=-0.62$, $P<0.001$; MTT: $R=0.59$, $P<0.001$). Among the Xe129 gas uptake measurements, RBC-to-gas ratios had more significant correlations with perfusion measurements as compared to tissue-to-gas and RBC-to-tissue ratios. Not surprisingly, %VD showed strong negative correlations with all gas uptake measurements including tissue-to-gas ratio ($R=-0.51$, $P<0.001$), RBC-to-gas ratio ($R=-0.64$, $P<0.001$) and RBC-to-tissue ratio ($R=-0.67$, $P=0.005$).

Patterns of Functional Abnormalities

Five distinctive patterns of functional abnormalities were found in patients with For the first three cases (Area 1–3, Figure 2), consistent results were seen among chest CT, perfusion MRI and Xe129 MRI. However, in the latter two cases (Area 4 and 5, Figure 3), low gas exchange was found with Xe129 MRI but was not identified on chest CT or perfusion MRI. The first area (Area 1, Figure 2) exhibited the combination of emphysematous lung by chest CT, low perfusion (i.e., low MRI PBV), poor ventilation (high $\%V_D$), and poor gas exchange (i.e., low Xe129 RBC-to-gas ratios). The second area (Area 2, Figure 2) exhibited normal lung tissue without emphysema by chest CT, but nonetheless had low perfusion, poor ventilation and poor gas exchange (low Xe129 RBC-to-gas ratios). The major difference

between Areas 1 and 2 was the divergent appearance of tissue destruction found by chest CT, with clearly abnormal perfusion and gas exchange found by MRI. The third area (Area 3, Figure 2) exhibited normal lung tissue without emphysema by chest CT and normal ventilation, but low perfusion and poor gas exchange. Thus this area appeared normal by chest CT, and was well ventilated, but had a fissure-like perfusion defect, and abnormally low gas uptake as measured by Xe129 DP MRI. The fourth area (Area 4, Figure 3) exhibited normal lung tissue without emphysema by chest CT and normal perfusion, but had poor ventilation and poor gas exchange. The fifth area (Area 5, Figure 3) had normal lung tissue without emphysema on chest CT, and normal perfusion and normal ventilation on MRI. Xe129 gas reached the lung tissue phase (i.e., normal tissue-to-gas ratios), but did not reach the blood phase (i.e., low RBC-to-gas ratios).

DISCUSSION

In this pilot study, we investigated pulmonary morphology and function in the lungs of patients with COPD by measuring tissue density with CT, pulmonary perfusion with Gd-enhanced perfusion MRI, and ventilation and gas uptake with hyperpolarized Xe129 MRI. A lobar segmentation method for MRI enabled us to perform regional analysis of lung function and to quantitatively compare imaging results from the different imaging modalities.

Several key points emerged from analysis of the data. First, all imaging modalities could differentiate the lungs of patients with COPD from those of AMN. The CT Perc15, MRI PBF, Xe129 MRI $\%V_D$, and the three parameters from the Xe129 gas uptake MRI were significantly different between patients with COPD and AMN. Second, tissue integrity, reflected by the tissue density from the chest CT, correlated with pulmonary perfusion, ventilation, and Xe129 dissolved in the lung tissue and RBCs. Third, pulmonary perfusion was significantly correlated with the severity of ventilation abnormalities (%VD). Fourth, quantitative imaging parameters revealed different patterns of pulmonary physiology in patients with COPD. Xe129 ventilation and gas uptake MRI provided additional information, beyond that provided by chest CT and Gd-enhanced MRI, necessary to fully understand COPD-associated pathophysiology. For example, for the cases shown in Figure 3, neither chest CT nor perfusion MRI could identify regional airflow limitation (Area 4) or potential impairment of gas exchange without reduced ventilation or perfusion (Area 5). Nonetheless, by using only the Xe129 DP MRI technique without perfusion imaging, r, we were not able to identify whether reduced gas exchange from interstitial tissue to blood results from reduced pulmonary perfusion (Area 3, Figure 2) or from impairment of gas exchange pathways (Area 5,Figure 3). These results demonstrated that combining multiple imaging modalities enabled us to further refine our understanding of the pathophysiology found in the lungs of patients with COPD.

Imaging results, such as those shown in Figure 2 and 3, further demonstrated the inter-connectedness and usefulness of all imaging modalities, and highlighted how these modalities can reveal features of *in-vivo* pulmonary physiology pertinent to COPD. In this regard, there were also several important observations noted in this study which merit additional discussion. First, significant correlation between CT Percl5 and the Xel29 tissue-to-gas ratio ($R=0.74$, $P<0.001$) was expected because these measurements represent

pulmonary tissue density and severity of emphysema. The Xel29 RBC-to-gas ratio was also highly correlated with CT Perc15 (R=0.68, P<0.001). The Xel29 RBC-to-gas ratio can be affected by emphysematous tissue destruction in two ways. Emphysema and/or hyper-expansion of the lung would decrease CT Percl5 values by vascular pruning and/or vessel compression at the microvascular level (30). These changes would likely decrease pulmonary perfusion and thus the RBC-to-gas ratio. The Xel29 RBC-to-gas ratio would also be directly affected by changes in gas uptake through the lung tissue (tissue-to-gas ratio). A good example of this was seen in the Area 1 of subject C4, shown in Figure 2. With sever emphysema, Area 1 was suspected to have very little functioning tissue left as HRCT. Both ventilation (Xel29 “gas” image) and perfusion (PBV) were very low, which would have likely led to virtually no gas uptake in this area.

Second, pulmonary perfusion was correlated with $\%V_D$ (PBV: R=−0.59, PBF: R=−0.62, MTT: R=0.59; all P<0.001) more significantly than with CT Perc15 (PBV: R=0.38, P=0.016; PBF: R=0.42, P=0.007; MTT: R=−0.36, P=0.022). This may mean perfusion variation from compensatory vasoconstriction response to ventilation changes to maintain V/Q coupling (31) dominates vascular pruning or hyper-expansion detectable by CT. A supporting example was Area 2 from subject C4 shown in Figure 2. Lung tissue in the Area 2 appears to be intact based on CT, but ventilation and PBF were abnormally low. It is not surprising that strong correlations were found between $\%V_d$ and gas uptake measurements, since the first requirement for a functional region to uptake gas is to be ventilated. The stronger correlations of $\%V_D$ with RBC-to-gas and RBC-to-tissue ratios than with tissue-to-gas ratios also supported the inter-connections between ventilation and perfusion in these subjects as discussed above.

Third, it is worthwhile to note that the Xel29 RBC-to-gas ratio, an imaging counterpart of DLCO, correlated strongly with CT Percl5 (R=0.62, P<0.001), perfusion (e.g. MTT: R=−0.52, P<0.001) and ventilation (R=−0.64, P<0.001). As a measurement of gas exchange efficiency along the complete pathway from the alveolar airspace to blood in the lung, the Xel29 RBC-to-gas ratio should be dependent upon changes in ventilation, perfusion, gas exchange, or tissue density.RBC-to-gas ratio is likely reduced for two situations (or certainly combination of the two); in pulmonary “shunt,” with normal perfusion and abnormal ventilation, and in “dead space,” with normal ventilation and abnormal perfusion. Our preliminary study clearly showed these two circumstances. A big ventilation defect in Area 4 was accompanied by normal perfusion on the PBF map and normal lung tissue density on CT, a case of shunt. The underlying mechanism for Area 4 could be airway obstruction associated with chronic bronchitis (6) without destruction of lung tissue and blood vessels. By contrast, normally ventilated Area 3 in Figure 2 was accompanied by a prominent fissure-like perfusion defect and a low RBC-to-gas ratio in the middle of the left lung. The underlying mechanism for Area 3 could be a pathologic process limited to the pulmonary blood vessels (6) without abnormal airflow or loss of lung parenchyma.

Fourth, RBC-to-tissue ratios primarily reflect pulmonary perfusion and gas exchange efficiency from interstitial tissue to blood.As expected, the RBC-to-tissue ratio was significantly lower in COPD (P<0.001), but this parameter was only moderately correlated with perfusion measurements (PBV: R=0.35, P=0.028; PBF: R=0.38, P=0.015; MTT: R=

−0.48, P=0.002). This suggests that the gas exchange efficiency may be dependent on other physiological factors such as alveolar septal wall thickness and integrity, which was shown be significantly altered in COPD (12, 32). Area 5 in Figure 3 provides evidences that strongly supported this hypothesis.

Finally, low CT Perc15 and Xe129 tissue-to-gas ratios in the right middle lobe were mostly due to lower tissue density in the right middle lobe compared to other lobes. Anatomically the right middle lobe resides in the anterior part of the body. In our study, subjects were imaged in supine position, which may have caused compression of posterior lung tissue due to gravity. Interestingly, this trend disappeared in the COPD group. We speculate that emphysema or hyper-expansion of the lung in patients with COPD could have reduced lung tissue elasticity, suppressing the lung's response to gravity with postural change, consistent with other group's findings (33, 34).

Our study is limited in several ways. First, a small number of subjects participated in our pilot study, and thus our statistical results should be interpreted with caution. Even though our lobar segmentation method enabled us to separate the lungs into individual lobes and to analyze relationship among different imaging acquisitions quantitatively, the functional alterations of the lung found in COPD patients may be biased. Therefore, we are currently conducting studies in additional subjects to confirm the results of this pilot study. Second, biological variation in pulmonary physiology is anticipated within a subject as well as between subjects. Further, longitudinal studies will help to validate the complex morphologic and functional changes observed. Third, while the heterogeneity of pulmonary physiology observed in some of the subjects is highly intriguing, observations from more control subjects are necessary. For example, pulmonary physiology of patients with homogeneous emphysema and patients with pure chronic bronchitic airway disease can serve as excellent positive control subjects for future studies.

In conclusion, by using chest CT, Gd-enhanced perfusion MRI, and Xel29 tion and gas uptake MRI, we assessed the quantitative changes in tissue density, pulmonary perfusion and gas uptake in patients with COPD as compared to age matched normal subjects. We found evidence for compensatory pulmonary vasoconstriction to match impairment of ventilation, and also pulmonary shunt and dead space. Furthermore, by incorporating a new lobar segmentation method for proton MRI, we were able to perform statistical analysis to evaluate the regional interrelationships of Xe129 gas uptake measurements with tissue density, perfusion, and ventilation. We demonstrated that Xe129 MRI has high potential to identify changes of multiple aspects of lung physiology in one acquisition not assessable by other existing imaging methods.

ACKNOWLEDGEMENT:

This work is supported by NIH (R21HL129112, R01HL109618, R01HL132287, and R01HL132177 from the National Heart, Lung, and Blood Institute) and research funding from Siemens Medical Solutions. Also the authors sincerely appreciate the organization of the 2017 International Workshop on Pulmonary Imaging held at the University of Pennsylvania, and the opportunity for publication on Academic Radiology.

Funding Source: NIH (R21HL129112, R01HL109618, R01HL132287, and R01HL132177 from the National Heart, Lung, and Blood Institute), and research funding from Siemens Medical Solutions

References:

1. Kim V, Han MK, Vance GB, Make BJ, Newell JD, Hokanson JE, Hersh CP, Stinson D, Silverman EK, Criner GJ, Investigators CO. The chronic bronchitic phenotype of COPD: an analysis of the COPDGene Study. Chest 2011; 140: 626–633. [PubMed: 21474571]
2. Vestbo J, Agusti A, Wouters EF, Bakke P, Calverley PM, Celli B, Coxson H, Crim C, Edwards LD, Locantore N, Lomas DA, MacNee W, Miller B, Rennard SI, Silverman EK, Yates JC, Tal-Singer R, Evaluation of CLtIPSESI. Should we view chronic obstructive pulmonary disease differently after ECLIPSE? A clinical perspective from the study team. American journal of respiratory and critical care medicine 2014; 189: 1022–1030. [PubMed: 24552242]
3. Cosio MG, Guerassimov A. Chronic obstructive pulmonary disease. Inflammation of small airways and lung parenchyma. American journal of respiratory and critical care medicine 1999; 160: S21–25. [PubMed: 10556164]
4. Rodriguez-Roisin R, Drakulovic M, Rodriguez DA, Roca J, Barbera JA, Wagner PD. Ventilation-perfusion imbalance and chronic obstructive pulmonary disease staging severity. Journal of applied physiology 2009; 106: 1902–1908. [PubMed: 19372303]
5. Rabe KF, Hurd S, Anzueto A, Barnes PJ, Buist SA, Calverley P, Fukuchi Y, Jenkins C, Rodriguez-Roisin R, van Weel C, Zielinski J, Global Initiative for Chronic Obstructive Lung D. Global strategy for the diagnosis, management, and prevention of chronic obstructive pulmonary disease: GOLD executive summary. American journal of respiratory and critical care medicine 2007; 176: 532–555. [PubMed: 17507545]
6. Kent BD, Mitchell PD, McNicholas WT. Hypoxemia in patients with COPD: cause, effects, and disease progression. International journal of chronic obstructive pulmonary disease 2011; 6: 199–208. [PubMed: 21660297]
7. Young IH, Bye PT. Gas exchange in disease: asthma, chronic obstructive pulmonary disease, cystic fibrosis, and interstitial lung disease. Comprehensive Physiology 2011; 1: 663–697. [PubMed: 23737199]
8. Sverzellati N, Molinari F, Pirronti T, Bonomo L, Spagnolo P, Zompatori M. New insights on COPD imaging via CT and MRI. International journal of chronic obstructive pulmonary disease 2007; 2: 301–312. [PubMed: 18229568]
9. Fornaro J, Leschka S, Hibbeln D, Butler A, Anderson N, Pache G, Scheffel H, Wildermuth S, Alkadhi H, Stolzmann P. Dual- and multi-energy CT: approach to functional imaging. Insights into imaging 2011; 2: 149–159. [PubMed: 22347944]
10. Roach PJ, Schembri GP, Bailey DL. V/Q scanning using SPECT and SPECT/CT. Journal of nuclear medicine 2013; 54: 1588–1596. [PubMed: 23907760]
11. Qing K, Ruppert K, Jiang Y, Mata JF, Miller GW, Shim YM, Wang C, Ruset IC, Hersman FW, Altes TA, Mugler JP, 3rd, Regional mapping of gas uptake by blood and tissue in the human lung using hyperpolarized xenon-129 MRI. Journal of magnetic resonance imaging 2014; 39: 346–359. [PubMed: 23681559]
12. Qing K, Mugler JP, 3rd, Altes TA, Jiang Y, Mata JF, Miller GW, Ruset IC, Hersman FW, Ruppert K. Assessment of lung function in asthma and COPD using hyperpolarized 129Xe chemical shift saturation recovery spectroscopy and dissolved-phase MRI. NMR in biomedicine 2014; 27: 1490–1501. [PubMed: 25146558]
13. Kaushik SS, Robertson SH, Freeman MS, He M, Kelly KT, Roos JE, Rackley CR, Foster WM, McAdams HP, Driehuys B. Single-breath clinical imaging of hyperpolarized (129)Xe in the airspaces, barrier, and red blood cells using an interleaved 3D radial 1-point Dixon acquisition. Magnetic resonance in medicine 2016; 75:1434–1443. [PubMed: 25980630]
14. Dregely I, Mugler JP, 3rd, Ruset IC, Altes TA, Mata JF, Miller GW, Ketel J, Ketel S, Distelbrink J, Hersman FW, Ruppert K. Hyperpolarized Xenon-129 gas-exchange imaging of lung microstructure: first case studies in subjects with obstructive lung disease. Journal of magnetic resonance imaging 2011; 33: 1052–1062. [PubMed: 21509861]
15. Kaushik SS, Freeman MS, Yoon SW, Liljeroth MG, Stiles JV, Roos JE, Foster W, Rackley CR, McAdams HP, Driehuys B. Measuring diffusion limitation with a perfusion-limited gas--hyperpolarized 129Xe gas-transfer spectroscopy in patients with idiopathic pulmonary fibrosis. Journal of applied physiology 2014; 117: 577–585. [PubMed: 25038105]

16. Vestbo J, Hurd SS, Agusti AG, Jones PW, Vogelmeier C, Anzueto A, Barnes PJ, Fabbri LM, Martinez FJ, Nishimura M, Stockley RA, Sin DD, Rodriguez-Roisin R. Global strategy for the diagnosis, management, and prevention of chronic obstructive pulmonary disease: GOLD executive summary. American journal of respiratory and critical care medicine 2013; 187: 347–365. [PubMed: 22878278]

17. Labaki WW, Martinez CH, Martinez FJ, Galban CJ, Ross BD, Washko GR, Barr RG, Regan EA, Coxson HO, Hoffman EA, Newell JD, Jr., Curran-Everett D, Hogg JC, Crapo JD, Lynch DA, Kazerooni EA, Han MK. The Role of Chest Computed Tomography in the Evaluation and Management of the Patient with COPD. American journal of respiratory and critical care medicine 2017.

18. Kim S, Jacob JS, Kim DC, Rivera R, Lim RP, Lee VS. Time-resolved dynamic contrast-enhanced MR urography for the evaluation of ureteral peristalsis: initial experience. Journal of magnetic resonance imaging 2008; 28: 1293–1298. [PubMed: 18972340]

19. Wild JM, Ajraoui S, Deppe MH, Parnell SR, Marshall H, Parra-Robles J, Ireland RH. Synchronous acquisition of hyperpolarised 3He and 1H MR images of the lungs - maximising mutual anatomical and functional information. NMR in biomedicine 2011; 24: 130–134. [PubMed: 20821726]

20. Qing K, Altes TA, Tustison NJ, Mata JF, Miller GW, Tobias WA, Cates GD, Brookeman JR, Mugler JP, 3rd. Acquisition of spatially-registered helium-3 and proton 3D image sets of the lung in less than 10 seconds using compressed sensing (abstract). Proc Intl Soc Mag Reson Med 19; 2011 p. 1349.

21. Tustison NJ, Qing K, Wang C, Altes TA, Mugler JP, 3rd., Atlas-based estimation of lung and lobar anatomy in proton MRI. Magnetic resonance in medicine 2016; 76: 315–320. [PubMed: 26222827]

22. Dijkstra AE, Postma DS, ten Hacken N, Vonk JM, Oudkerk M, van Ooijen PM, Zanen P, Mohamed Hoesein FA, van Ginneken B, Schmidt M, Groen HJ. Low-dose CT measurements of airway dimensions and emphysema associated with airflow limitation in heavy smokers: a cross sectional study. Respiratory research 2013; 14: 11. [PubMed: 23356533]

23. Mets OM, van Hulst RA, Jacobs C, van Ginneken B, de Jong PA. Normal range of emphysema and air trapping on CT in young men. AJR American journal of roentgenology 2012; 199: 336–340. [PubMed: 22826394]

24. Mohamed Hoesein FA, de Hoop B, Zanen P, Gietema H, Kruitwagen CL, van Ginneken B, Isgum I, Mol C, van Klaveren RJ, Dijkstra AE, Groen HJ, Boezen HM, Postma DS, Prokop M, Lammers JW. CT-quantified emphysema in male heavy smokers: association with lung function decline. Thorax 2011; 66: 782–787. [PubMed: 21474499]

25. Ohno Y, Hatabu H, Murase K, Higashino T, Kawamitsu H, Watanabe H, Takenaka D, Fujii M, Sugimura K. Quantitative assessment of regional pulmonary perfusion in the entire lung using three-dimensional ultrafast dynamic contrast-enhanced magnetic measurement of blood flow and volume. J Appl Physiol 1954; 6: 731–744. [PubMed: 13174454]

26. Meier P, Zierler KL. On the theory of the indicator-dilution method for measurement of blood flow and volume. J Appl Physiol 1954; 6: 731–744 [PubMed: 13174454]

27. Zierler K Indicator dilution methods for measuring blood flow, volume, and other properties of biological systems: a brief history and memoir. Annals of biomedical engineering 2000; 28: 836–848. [PubMed: 11144667]

28. Tustison NJ, Avants BB, Flors L, Altes TA, de Lange EE, Mugler JP, 3rd, Gee JC. Ventilation-based segmentation of the lungs using hyperpolarized (3)He MRI. Journal of magnetic resonance imaging 2011; 34: 831–841. [PubMed: 21837781]

29. Qing K, Altes TA, Tustison NJ, Feng X, Chen X, Mata JF, Miller GW, de Lange EE, Tobias WA, Cates GD, Jr., Brookeman JR, Mugler JP, 3rd. Rapid acquisition of helium-3 and proton three-dimensional image sets of the human lung in a single breath-hold using compressed sensing. Magnetic resonance in medicin 2015; 74:

30. Rahaghi FN, van Beek EJ, Washko GR. Cardiopulmonary coupling in chronic obstructive pulmonary disease: the role of imaging. Journal of thoracic imaging 2014; 675–691.

31. Stenmark KR, Fagan KA, Frid MG. Hypoxia-induced pulmonary vascular remodeling: cellular and molecular mechanisms. Circulation research 2006; 99: 675–691. [PubMed: 17008597]

32. Ruppert K, Qing K, Altes TA, Mata JF, Ruset IC, Hersman FW, Mugler JP. Septal Wall Thickness Changes In COPD Assessed By CSSR MR Spectroscopy. D19 MR AND MRS: IMAGING REGIONAL LUNG FUNCTION. p. A5419–A5419.

33. Cleveland ZI, Cofer GP, Metz G, Beaver D, Nouls J, Kaushik SS, Kraft M, Wolber J, Kelly KT, McAdams HP, Driehuys B. Hyperpolarized Xe MR imaging of alveolar gas uptake in humans. PloS one 2010; 5: e12192. [PubMed: 20808950]

34. Mugler JP, 3rd, Driehuys B, Brookeman JR, Cates GD, Berr SS, Bryant RG, Daniel TM, de Lange EE, Downs JH, 3rd, Erickson CJ, Happer W, Hinton DP, Kassel NF, Maier T, Phillips CD, Saam BT, Sauer KL, Wagshul ME. MR imaging and spectroscopy using hyperpolarized 129Xe gas: preliminary human results. Magnetic resonance in medicine 1997; 37: 809–815. [PubMed: 9178229]

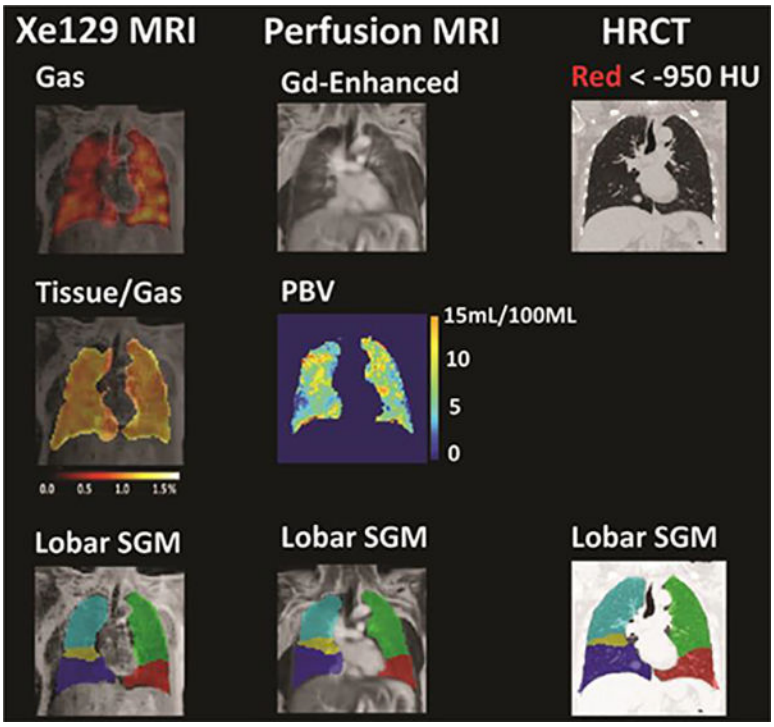

Figure 1.

Representative lobar segmentation of Xel29 MRI, Gd-enhanced perfusion MRI, and CT images. Left column: top row: ventilation image ("Gas") overlaid on proton image acquired in the same breath hold as Xe129 images; middle row: generated tissue-to-gas ratio map on top of proton image; bottom row: lobar segmentation for proton image acquired with Xel29 MRI acquisition. Middle column: top row: Gd-enhanced perfusion MRI image of the lung; middle row: generated pulmonary blood volume map (PBV) in the lung region; bottom row: lobar segmentation for Gd-enhanced perfusion MRI image. Right column: top row: high resolution CT image of the lung with regions lower than −950 HU marked by red dots; bottom row: lobar segmentation for CT was done based on the fissure detected. Images showed a representative slice of the 3-D Xe129, Gd-enhanced perfusion MRI and HRCT acquisitions from approximately the same position of the lung.

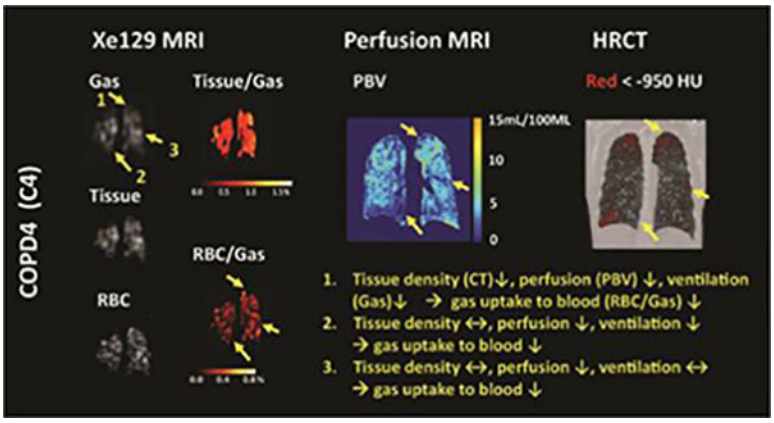

Figure 2.

Representative CT image, PBV, and Xe129 tissue-to-gas and RBC-to-gas ratio maps from subject C4 and C2. Alterations of lung function exhibited different patterns in the lung, as shown in areas 1–4 in the figure. The RBC-to-gas ratio measured by Xe129 MRI reflecting overall gas exchange to the blood was found to be low in concordance with low tissue density measured by CT (area 1), low perfusion measured by perfusion MRI (area 3), or the combination of both (area 2).

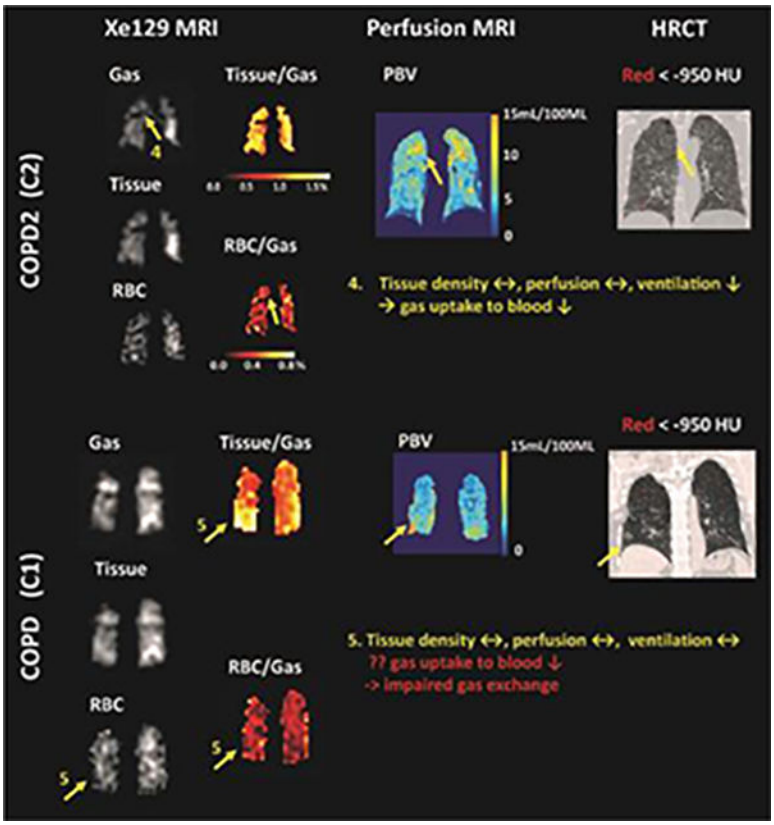

Figure 3.

Representative CT images, PBV maps, and Xe129 tissue-to-gas and RBC-to-gas ratio maps from subject C1 and C2 showed that Xe129 MRI could uniquely detect low gas exchange to blood by either low gas ventilation (area 4) or potentially impaired gas exchange from lung tissue to the blood (area 5). This information was not accessible by perfusion MRI or CT.

Table 1.

Subject demographics and PFT results

	Sex	Age	FEV1/ FVC	FEV1 %Pred	DLCO %Pred	DLCO/Va %Pred	6MW
H1	F	**52***	**91**	**111**	91	93	**587**
H2	F	61	**74**	106	82	**77**	487
H3	F	60	83	**93**	**93**	**114**	**442**
H4	F	**62***	79	99	**77**	78	450
C1	F	**66**	59	62	60	75	424
C2	F	**56**	**69**	63	**85**	**96**	425
C3	M	64	57	**80**	77	76	**495**
C4	M	58	**24**	**25**	**44**	**49**	**225**

*Bold means upper limit for measurements in each group (healthy or COPD group); Bold+underline means lower limit for measurement in each group

Table 2.

Whole-lung average measurements obtained from imaging acquisitions

	CT	*Gd-MRI*				*HP Xe129 MRI*		
	Perc15	**PBV**	**PBF**	**MTT**	**%Vd**	**Tissue /Gas**	**RBC /Gas**	**RBC /Tissue**
H1	−881	6.6	77	8.9	21	0.95	**0.34**	**0.35**
H2	**−889***	**11.4**	**135**	8.4	**14**	**0.79**	0.28	0.27
H3	**−833***	8.7	118	**8.3**	31	0.92	0.28	**0.20**
H4	−849	**5.9**	**68**	**9.6**	**36**	**1.06**	**0.26**	0.21
C1	−897	**8.2**	**119**	**7.3**	**26**	**0.89**	0.23	**0.20**
C2	−884	6.7	69	10.1	38	0.85	**0.27**	0.18
C3	−905	7.8	80	9.1	34	0.36	0.21	0.18
C4	**−941**	**3.6**	**30**	**11.9**	**62**	**0.25**	**0.15**	**0.11**

*Bold means upper limit for measurements in each group (healthy or COPD group); Bold+underline means lower limit for measurement in each group

Table 3.

Comparison of lobar mean values from AMN and COPD groups[a]

		CT	Gd-MRI			HPXe129 MRI			
		Perc15	PBV	PBF	MTT	%V_D	Tissue /Gas	RBC /Gas	RBC /Tissue
AMN	1[b]	**−843***	**9.1**	**108**	**9.0**	29	1.06	0.29	0.26
	2	−876	8.0	96	9.0	21	0.92	0.25	0.24
	3	−848	7.9	100	**8.4**	26	1.01	0.29	0.28
	4	**−890***	**6.6**	**79**	8.9	24	0.74	0.23	0.28
	5	−872	8.2	100	8.8	28	0.82	0.25	0.25
P_Lob[b]		0.12	0.61	0.67	0.81	0.90	0.18	0.42	0.95
COPD	1	−892	6.7	75	9.4	**35**	**0.65**	**0.18**	**0.18**
	2	**−924**	6.4	74	9.8	**44**	0.60	0.16	0.16
	3	**−887**	**7.1**	75	**9.9**	40	0.59	0.16	**0.15**
	4	−919	**5.9**	**68**	**9.4**	36	0.55	**0.15**	0.18
	5	−915	6.5	**77**	9.6	41	**0.53**	0.15	0.17
P_Lob		0.24	0.99	0.99	0.98	0.99	0.95	0.86	0.87
P_Grp[d]		**<0.001**	0.19	**0.047**	0.07	**0.006**	**<0.001**	**<0.001**	**<0.001**

[a.] Units for measurements are CT Perc15: HU; Gd-MRI PBV: mL/100 mL, PBF: mL/100mL/min

[b.] Lobe 1: left lower, 2: left upper, 3: right lower, 4: right middle, 5: right upper

c. P values for one-way Kruskal-Wallis to analyze the differences among lobes

[d.] P values for Mann-Whitney U test to compare the AMN and COPD groups

[e.] *Bold means upper limit for measurements in each group (healthy or COPD group); Bold+underline means lower limit for measurement in each group

Table 4.

Correlation between different imaging measurements

	GD-MRI				XE129 MRI		
	PBV	**PBF**	**MTT**	**%V_d**	**Tissue /Gas**	**RBC /Gas**	**RBC /Tissue**
CT	0.38(R)*	0.42	−0.36	−0.33	**0.74**	**0.62**	0.26
PERC15	0.016(P)*	0.007	0.022	0.04	**<0.001**	**<0.001**	0.10
PBV	--	--	--	**−0.59**	0.37	0.42	0.35
				<0.001	*0.018*	0.007	0.028
PBF	--	--	--	**−0.62**	0.48	0.49	0.38
				<0.001	0.002	0.002	0.015
MTT	--	--	--	**0.59**	−0.45	**−0.52**	−0.48
				<0.001	0.004	**<0.001**	0.002
$\%V_D$				--	**−0.51**	**−0.64**	**−0.67**
					<0.001	**<0.001**	**<0.001**

*R: non-parametric correlation coefficient (upper row of each item). P: p value of the correlation.